energies

MDPI

Article

Low-Carbon Optimal Scheduling of RIES Considering Source-Load Coordination Under Green Certificate and Carbon Trading

Pengfei Cao [1] and Jundong Duan [2,*]

[1] School of Electrical Engineering and Automation, Henan Polytechnic University, Jiaozuo 454000, China; 212407020128@home.hpu.edu.cn

[2] Key Laboratory of Intelligent Detection and Control of Coal Mine Equipment in Jiaozuo, Jiaozuo 454003, China

* Correspondence: jundongd@hpu.edu.cn

Abstract

To achieve efficient clean energy accommodation and low-carbon economic operation of regional integrated energy systems (RIES), this paper proposes an optimal scheduling strategy that considers source–load coordination and a joint green certificate–stepped carbon trading mechanism. On the source side, a deeply coupled model integrating combined heat and power (CHP), carbon capture and storage (CCS), and two-stage power-to-gas (P2G) (collectively termed CCP) is established to enable autonomous carbon recycling within the system. On the load side, taking into account the regulation characteristics of multiple loads, a multi-energy demand response model is developed to unlock the scheduling potential of the demand side. At the market mechanism level, a joint green certificate–stepped carbon trading mechanism is constructed as an external signal to incentivize clean energy consumption. Finally, an optimal RIES scheduling model is formulated with the objective of minimizing the total comprehensive cost, and the problem is solved using the CPLEX solver via MATLAB R2023b. Comparative results under different scenarios demonstrate that the proposed strategy effectively enhances clean energy accommodation rates, reduces carbon emissions, and achieves low-carbon economic operation of the system.

Keywords: regional integrated energy system; green certificate trading; renewable energy consumption; multi-energy demand response; low-carbon economy

1. Introduction

In recent years, greenhouse gas emissions have been on the rise, and global climate warming is becoming increasingly severe [1,2]. As the primary source of global greenhouse gas emissions, the energy sector has become a critical link in carbon emission reduction [3]. A single type of low-carbon energy technology is insufficient to address current carbon emission challenges, necessitating the consideration of coupling, complementarity, and synergy among multiple energy sources. Integrated energy systems (IES) can achieve efficient energy utilization and have gradually become a key means of promoting the low-carbon energy transition [4].

To promote the marketization of renewable energy, China has established the renewable portfolio standard (RPS), of which the green certificate trading (GCT) mechanism is a direct product [5]. Some scholars have conducted respective studies on the car-

Academic Editor: Brian D. Fath

Received: 2 October 2026
Revised: 19 November 2026
Accepted: 24 November 2026
Published: 28 November 2026

Copyright: © 2026 by the authors. Licensee MDPI, Basel, Switzerland. This article is an open access article distributed under the terms and conditions of the Creative Commons Attribution (CC BY) license.

bon emission trading (CET) and GCT mechanisms. Literature [6] verified that a ladder-type CET mechanism considering CET costs can most effectively control both economic and environmental levels. In literature [7–9], the authors demonstrated an interactive and mutually reinforcing relationship between the green certificate market and the electricity market, whose coordinated development exerts a positive impact on the structural adjustment of China's power supply, with renewable energy quota targets acting as a key influencing factor. Literature [10] comprehensively considered both CET and GCT market mechanisms to ensure the economic and low-carbon operation of virtual power plants. Integrating these two market mechanisms can effectively balance the system's economic and low-carbon objectives.

Currently, traditional power systems face limitations in multiple aspects, making it difficult to fully unleash their low-carbon potential. To address this, scholars have proposed regional integrated energy systems (RIES) and, based on RIES, investigated how to utilize carbon resources to further enhance the system's carbon mitigation capability. Literature [11] introduced carbon capture and storage (CCS) into RIES and established a carbon capture model. Literature [12] integrated CCS with power-to-gas (P2G) to resolve challenges faced by integrated electricity–gas systems in energy consumption and low-carbon economic operation. Literature [13] considered "carbon coupling" and "electricity-gas coupling" by introducing P2G equipment, thereby achieving significant low-carbon economic benefits. Literature [14] accounted for the dynamic characteristics of gas and heating networks, and constructed a comprehensive flexible operation model for carbon capture power plants alongside a two-phase refined P2G model, effectively improving system economics and reducing carbon emission levels. In literature [15,16], considering the coupling characteristics of multiple loads, an RIES model incorporating electricity–heat–gas integrated demand response (IDR) was proposed, with results indicating that the application of IDR can promote the low-carbon and economic development of RIES. Furthermore, literature [17,18] proposed a P2G-CCS low-carbon optimization model coupling CCS with power-to-gas, achieving a higher level of carbon emission reduction; however, they failed to fully exploit the bidirectional flexibility of the source–load interaction.

In summary, existing studies have explored the low-carbon potential of power systems from three dimensions: the source side, storage side, and load side. Although these efforts have enhanced renewable energy accommodation and reduced carbon emissions, they also increased system operating costs due to the introduction of additional units. Furthermore, the aforementioned studies lack sufficient depth in exploring the low-carbon potential of coordinated scheduling across various system links and the coupled operation of units, leaving room for further improvement in the bidirectional operational flexibility of the source–load interaction. To this end, this paper first constructs a combined heat and power (CHP)–carbon capture and storage (CCS)–two-stage power-to-gas (P2G) (CCP) coupling model on the source side. Second, considering the regulation capabilities of electricity, heat, and gas loads, a multi-energy demand response model is established. On this basis, a low-carbon economic dispatch model for regional integrated energy systems is formulated by incorporating the green certificate–ladder-type carbon joint trading mechanism. Finally, targeting the minimization of total system costs, the model is solved using CPLEX, and the proposed dispatching scheme is investigated and analyzed through multi-scenario comparisons. The main contributions of this paper are summarized as follows:

(1) Deeply coupled source-side carbon–energy recycling framework: A coordinated operation model integrating combined heat and power (CHP), carbon capture and storage (CCS), and two-stage power-to-gas (P2G) (termed the CCP framework) is

formulated. By capturing CO_2 emitted from the hydrogen-blended gas turbine to serve as a reliable feedstock for the methanation reactor (MR), this framework establishes a complete closed loop of carbon capture, conversion, and utilization, substantially reducing fuel procurement costs and easing wind curtailment.

(2) Market-driven bidirectional source–load coordination mechanism: A joint green certificate trading (GCT) and ladder-type carbon emission trading (CET) mechanism is introduced as an intermediary regulatory medium. Acting as external price signals, this joint mechanism bridges multi-energy integrated demand response (IDR) on the demand side with the CCP flexible output on the supply side, thereby unlocking bidirectional regulation flexibility and smoothing peak-to-valley load differences.

(3) Flexible demand-side multi-energy synergy via IDR: Through the modeling of diverse loads, the demand-side IDR mechanism guides loads to achieve temporal transfer and energy-form substitution, thereby reducing the peak–valley difference of loads, optimizing the multi-energy cooperative matching efficiency, and ultimately improving the overall system energy utilization rate and operational stability.

2. RIES Structure Incorporating CCP Coupling

2.1. Architecture of RIES

Regional integrated energy systems achieve efficient coordinated scheduling of energy supply, utilization, and storage by incorporating diverse energy carriers based on advanced intelligent management and optimal control techniques. Figure 1 depicts the framework of the RIES formulated in this study.

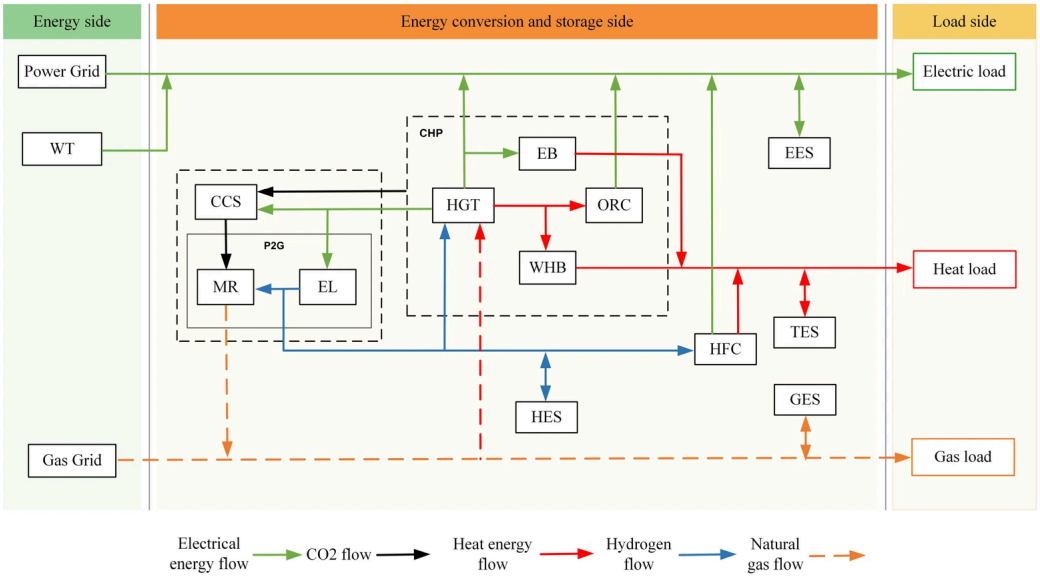

Figure 1. RIES framework diagram.

On the energy supply side, electrical energy is delivered by wind turbines (WT) and the upper-level power grid, while natural gas is supplied by the external gas network. On the energy conversion and coupling side, core facilities including combined heat and power (CHP), power-to-gas (P2G), and a hydrogen fuel cell (HFC) are integrated. By consolidating a hydrogen-blended gas turbine (HGT), an electric boiler (EB), an organic Rankine cycle (ORC), and a waste heat boiler (WHB), the CHP unit achieves thermoelectric decoupling alongside flexible dispatch. The P2G process is explicitly modeled as a two-stage conversion, wherein a carbon capture and storage (CCS) device provides the

necessary carbon source for the methanation reaction. On the energy storage side, a multi-carrier energy storage system encompassing four media is configured: battery (electrical energy storage, EES), thermal energy storage (TES) tank, gas energy storage (GES) tank, and hydrogen energy storage (HES) tank.

2.2. Coupled CCP Model

To deeply exploit the carbon emission reduction potential of the system, a collaborative operation model with CCP coupling is constructed to achieve the recycling and circular utilization of energy. The corresponding coupling mechanism is illustrated in Figure 2.

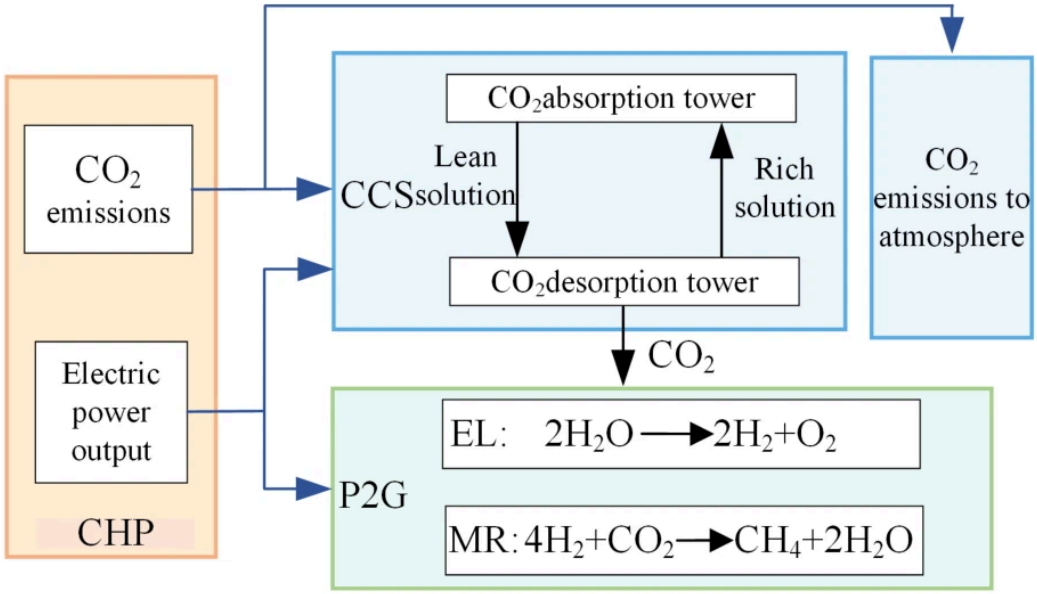

Figure 2. Coupling operation of CCP.

As shown in Figure 2, during the operation of the CHP unit, the CO_2 it emits is captured by the CCS facility to serve as the carbon source for the methanation reaction in the P2G process. Meanwhile, the electricity generated by the CHP unit is supplied to both the P2G and CCS facilities. Within the P2G system, an electrolytic cell (EL) consumes electricity to produce hydrogen, which then reacts with the captured CO_2 in a (methanation reactor, MR) to synthesize methane CH_4. This synthesized methane is subsequently fed back to fuel the CHP unit, enabling closed-loop internal carbon recycling. This mechanism not only reduces the system's external energy procurement costs but also plays a vital role in enhancing the low-carbon economic performance of the RIES.

2.2.1. Two-Stage P2G Modeling

Stage 1: The electrolytic cell (EL) converts electrical energy into hydrogen energy; Stage 2: The hydrogen and CO_2 react in the methanation reactor (MR) to synthesize methane. The corresponding mathematical formulations are established as follows:

$$\begin{cases} P_{\mathrm{EL,H}}(t) = \eta_{\mathrm{EL}} P_{\mathrm{e,EL}}(t) \\ P_{\mathrm{MR},\mathrm{CH_4}}(t) = \eta_{\mathrm{MR}} P_{\mathrm{H,MR}}(t) \end{cases} \quad (1)$$

where $P_{\mathrm{EL,H}}(t)$ denotes the hydrogen power output of the EL at time period t, kW; $P_{\mathrm{e,EL}}(t)$ represents the electric power consumed by the EL during time interval t, kW; and

η_{EL} is the conversion efficiency; where $P_{MR,CH_4}(t)$ is the methane power output of the MR at time period t, kW; $P_{H,MR}(t)$ represents the hydrogen power input to the MR during time interval t, kW; and η_{MR} denotes the energy conversion efficiency of the MR.

2.2.2. CCS Modeling

The operating power of the CCS during time interval t is denoted as $P_{CCS}(t)$, which comprises the base energy consumption $P_B(t)$ and the operational energy consumption $P_R(t)$.

$$\begin{cases} P_{CCS}(t) = P_R(t) + P_B(t) \\ E_S(t) = \eta_C C_{CO_2}(t) \\ P_R(t) = \lambda_e E_S(t) \end{cases} \tag{2}$$

where $E_S(t)$ is the amount of CO_2 captured by the CCS facility during time interval t, kg; $C_{CO_2}(t)$ is the carbon emissions of the gas turbine, kg; η_C denotes the carbon capture efficiency; λ_e is the specific energy consumption per unit of captured CO_2, kWh/t.

2.2.3. Flexible Output Model of CHP Unit

Traditional units struggle to dynamically adjust the optimal energy supply ratio according to demand [19]. In this paper, an organic Rankine cycle (ORC) and a waste heat boiler (WHB) are integrated into a combined heat and power (CHP) system to operate in coordination with an electric boiler (EB). The ORC utilizes waste heat for secondary power generation, the WHB satisfies the thermal load, and the EB leverages surplus grid electricity to supply heat. Working in concert, these three components establish a flexible output model for the CHP unit, thereby further improving its operational efficiency.

(1) Hydrogen-Blended Gas Turbine Modeling

Maintaining the hydrogen injection ratio into the gas turbine below 20% ensures the safe and stable operation of the burner [20]. Accordingly, the hydrogen blending ratio is set to 20% in this study. The specific mathematical model is formulated as follows:

$$\begin{cases} P_{HGT,e}(t) = \eta_{HGT,e}\left(P_{CH_4,HGT}(t) + P_{H,HGT}(t)\right) \\ P_{HGT,h}(t) = \eta_{HGT,h}\left(P_{CH_4,HGT}(t) + P_{H,HGT}(t)\right) \\ p^{min}_{CH_4,HGT} \le P_{CH_4,HGT}(t) \le p^{max}_{CH_4,HGT} \\ \tau_{HGT} = \dfrac{P_{H,HGT}(t)}{L^V_{H_2}} \left(\dfrac{P_{CH_4,HGT}(t)}{L^V_{CH_4}} + \dfrac{P_{H,HGT}(t)}{L^V_{H_2}} \right)^{-1} \end{cases} \tag{3}$$

where $P_{HGT,e}(t)$ and $P_{HGT,h}(t)$ denote the electrical and thermal power outputs of the HGT during time interval t, respectively, kW; $P_{CH_4,HGT}(t)$ and $P_{H,HGT}(t)$ represent the methane and hydrogen power inputs to the HGT during time interval t, respectively,

kW; $\eta_{HGT,e}$ and $\eta_{HGT,h}$ are the electricity and heat conversion efficiencies; $p^{max}_{CH_4,HGT}$ and $p^{min}_{CH_4,HGT}$ denote the upper and lower limits of the methane power input to the HGT, respectively, kW; τ_{HGT} is the hydrogen blending volume ratio; $L^{V}_{H_2}$ and $L^{V}_{CH_4}$ denote the volumetric calorific values of hydrogen and methane, KJ/m^3.

(2) Modeling of Other Equipment

The high-temperature flue gas discharged from the gas turbine is split in the waste heat header: a portion is directed to the WHB to satisfy the thermal load demand, while the remainder is fed into the ORC for waste heat power generation, thereby realizing the secondary conversion of thermal energy.

$$\begin{cases} P_{HGT,h}(t) = P_{h,WHB}(t) + P_{h,ORC}(t) \\ P_{WHB,h}(t) = \eta_{WHB} P_{h,WHB}(t) \\ P_{ORC,e}(t) = \eta_{ORC} P_{h,ORC}(t) \\ P_{EB,h}(t) = \beta_{EB} P_{e,EB}(t) \end{cases} \tag{4}$$

where $P_{h,WHB}(t)$, $P_{h,ORC}(t)$ denote the thermal power inputs to the WHB, ORC, during time interval t, respectively, kW; η_{WHB}, η_{ORC} represent the energy conversion efficiencies of the WHB, ORC, respectively; β_{EB} is the electrothermal conversion coefficient of the EB; $P_{WHB,h}(t)$, $P_{ORC,e}(t)$, and $P_{EB,h}(t)$ represent the thermal power output of the WHB, the electric power output of the ORC, and the thermal power output of the EB during time interval t, respectively, kW; and $P_{e,EB}(t)$ denotes the electric power input to the EB during time interval t, kW.

(3) CHP Energy Outputs

$$\begin{cases} P_{CHP,e}(t) = P_{HGT,e}(t) + P_{ORC,e}(t) - P_{e,EB}(t) - P_{CCS}(t) - P_{EL}(t) \\ P_{CHP,h}(t) = P_{WHB,h}(t) + P_{EB,h}(t) \end{cases} \tag{5}$$

where $P_{CHP,e}(t)$ and $P_{CHP,h}(t)$ denote the electrical and thermal power outputs of the CHP unit during time interval t, respectively, in kW.

2.2.4. Carbon Recycling Model of the CCP System

$$\begin{cases} E_S(t) = P^{C}_{CO_2,MR}(t) + P^{C}_{CO_2,S}(t) \\ \eta_{CO_2} P^{C}_{CO_2,MR}(t) = 1.968 P_{MR,CH_4}(t) (L^{V}_{CH_4})^{-1} \\ P_{CO_2}(t) = P^{C}_{CO_2,MR}(t)(1 - \eta_{CO_2}) \\ E'_{total} = \sum_{t=1}^{T} (E_{CO_2}(t) - E_S(t) + P_{CO_2}(t)) \end{cases} \tag{6}$$

where $P^{C}_{CO_2,MR}(t)$ denotes the amount of CO_2 injected into the MR during time interval

t, kg; η_{CO_2} is the conversion efficiency; $P_{CO_2}(t)$ represents the amount of underutilized CO_2 during the methanation process in the MR at time interval t, kg; and E'_{total} denotes the amount of CO_2 emitted from the system into the atmosphere, kg; $P^{C}_{CO_2,S}(t)$ is the amount of captured CO_2 directed for permanent storage.

3. Demand Response and GEC–Tiered Carbon Trading Modeling

3.1. Demand Response Modeling

To fully exploit the dispatch flexibility on the demand side, loads are classified into fixed loads, shiftable loads, and substitutable loads. Specifically, shiftable loads leverage temporal shifting characteristics to transfer energy consumption from peak periods to valley periods, thereby smoothing the load curve. Substitutable loads utilize multi-energy conversion equipment to achieve flexible switching between different energy carriers at the same time interval, exploiting the coupling and substitution relationships among multi-energy flows. The corresponding mathematical formulations are established as follows:

$$P_{i,L}(t)=P^{S}_{i,L}(t)+P^{P}_{i,L}(t)+P^{K}_{i,L}(t) \tag{7}$$

where i denotes the load type, including electrical, thermal, and gas loads, kW; $P_{i,L}(t)$ is the baseline value of type-i load during time interval t prior to IDR, kW; $P^{S}_{i,L}(t)$ represents the fixed load of type i at time interval t, kW; $P^{P}_{i,L}(t)$ and $P^{K}_{i,L}(t)$ denote the shiftable load and substitutable load of type i during time interval t, respectively, kW.

$$\begin{cases} P^{P}_{i,L}(t)=P^{P,0}_{i,L}(t)+\Delta P^{P}_{i,L}(t) \\ \Delta P^{P}_{i,L}(t)=P^{P}_{i,in}(t)-P^{P}_{i,out}(t) \\ 0\le P^{P}_{i,in}(t)\le K^{P}_{i,in}(t)P^{P,0}_{i,L}(t) \\ 0\le P^{P}_{i,out}(t)\le K^{P}_{i,out}(t)P^{P,0}_{i,L}(t) \\ K^{P}_{i,in}(t)+K^{P}_{i,out}(t)\le 1;\sum_{t=1}^{T}\Delta P^{P}_{i,L}(t)=0 \\ \Delta P^{P,min}_{i,L}\le \Delta P^{P}_{i,L}(t)\le \Delta P^{P,max}_{i,L}(t) \end{cases} \tag{8}$$

where $\Delta P^{P}_{i,L}(t)$ denotes the response capacity of type-i load participating in the IDR during time interval t, kW; $P^{P,0}_{i,L}(t)$ is the initial shiftable load of type i; $K^{P}_{i,in}(t)$ and $K^{P}_{i,out}(t)$ represent the state variables for the load shift-in and shift-out of type-i

shiftable load, respectively, kW; $P_{i,\mathrm{in}}^{\mathrm{P}}(t)$ and $P_{i,\mathrm{out}}^{\mathrm{P}}(t)$ are the shift-in and shift-out powers of type-*i* shiftable load during time interval *t*, respectively, kW; $\Delta P_{i,\mathrm{L}}^{P,\max}$ and $\Delta P_{i,\mathrm{L}}^{P,\min}$ represent the upper and lower ratio limits for type-*i* shiftable load, respectively, kW; $P_{i,\mathrm{in}}^{\mathrm{P}}(t)$ and $P_{i,\mathrm{out}}^{\mathrm{P}}(t)$ denote continuous decision variables

$$\begin{cases} P_{i,\mathrm{L}}^{\mathrm{K}}(t)=P_{i,\mathrm{L}}^{\mathrm{K},0}(t)+\Delta P_{i,\mathrm{L}}^{\mathrm{K}}(t) \\ \Delta P_{i,\mathrm{L}}^{\mathrm{K}}(t)=P_{i,\mathrm{in}}^{\mathrm{K}}(t)-P_{i,\mathrm{out}}^{\mathrm{K}}(t) \\ 0\le P_{i,\mathrm{in}}^{\mathrm{K}}(t)\le K_{i,\mathrm{in}}^{\mathrm{K}}(t)P_{i,\mathrm{L}}^{\mathrm{K},0}(t) \\ 0\le P_{i,\mathrm{out}}^{\mathrm{K}}(t)\le K_{i,\mathrm{out}}^{\mathrm{K}}(t)P_{i,\mathrm{L}}^{\mathrm{K},0}(t) \\ K_{i,\mathrm{in}}^{\mathrm{K}}(t)+K_{i,\mathrm{out}}^{\mathrm{K}}(t)\le 1;\sum_{i=1}^{3}\Delta P_{i,\mathrm{L}}^{\mathrm{K}}(t)=0 \\ \Delta P_{i,\mathrm{L}}^{\mathrm{K},\min}(t)\le \Delta P_{i,\mathrm{L}}^{\mathrm{K}}(t)\le \Delta P_{i,\mathrm{L}}^{\mathrm{K},\max}(t) \end{cases} \tag{9}$$

where $P_{i,\mathrm{L}}^{\mathrm{K},0}(t)$ is the baseline substitutable load of type *i*, kW; $\Delta P_{i,\mathrm{L}}^{\mathrm{K}}(t)$ denotes the response capacity of type-*i* substitutable load participating in the IDR during time interval *t*; $K_{i,\mathrm{in}}^{\mathrm{K}}(t)$ and $K_{i,\mathrm{out}}^{\mathrm{K}}(t)$ represent the state variables for substitution-in and substitution-out of type-*i* load, respectively, kW; $P_{i,\mathrm{in}}^{\mathrm{K}}(t)$ and $P_{i,\mathrm{out}}^{\mathrm{K}}(t)$ denote the substitution-in and substitution-out powers of type-*i* substitutable load during time interval *t*, respectively, kW; $\Delta P_{i,\mathrm{L}}^{\mathrm{K},\max}(t)$ and $\Delta P_{i,\mathrm{L}}^{\mathrm{K},\min}(t)$ represent the upper and lower limits of the substitutable load of type *i*, respectively, kW; $P_{i,\mathrm{in}}^{\mathrm{K}}(t)$ and $P_{i,\mathrm{out}}^{\mathrm{K}}(t)$ denote continuous decision variables.

3.2. Green Certificate Trading Mechanism

Green certificates serve as the core credential for evaluating the fulfillment of renewable energy consumption quotas by energy enterprises [21], with the mechanism illustrated in Figure 3. The system acquires corresponding green certificates based on its actual clean energy consumption. If the number of acquired certificates exceeds the quota requirement, the surplus certificates can be sold on the market for profit or utilized to offset carbon emissions. Conversely, if a deficit occurs, additional green certificates must be purchased to cover the shortfall, thereby increasing the green certificate acquisition costs.

$$\begin{cases} G_{\mathrm{n}} = \chi_{\mathrm{P}}\chi_{\mathrm{Z}}\sum_{t=1}^{T} P_{\mathrm{e,load}}(t) \\ G_{\mathrm{h}} = \chi_{\mathrm{Z}}\sum_{t=1}^{T} P_{\mathrm{wind}}(t) \\ R_{\mathrm{GCT}} = \alpha_{\mathrm{GCT}} G_{\mathrm{GCT}} \end{cases} \tag{10}$$

where G_{n} denotes the green certificate quota, (book); χ_{P} and χ_{Z} represent the green certificate quota coefficient and conversion coefficient, respectively; $P_{\mathrm{e,load}}(t)$ is the electrical load of the system at time t, kW; G_{h} is the number of green certificates acquired, book; G_{GCT} denotes the volume of green certificates traded in the market, book; $P_{\mathrm{wind}}(t)$ represents the wind power output at time t, kW; α_{GCT} is the unit price of green certificates, CNY/book; T is the dispatch scheduling cycle, h; R_{GCT} is the GCT revenue of the RIES.

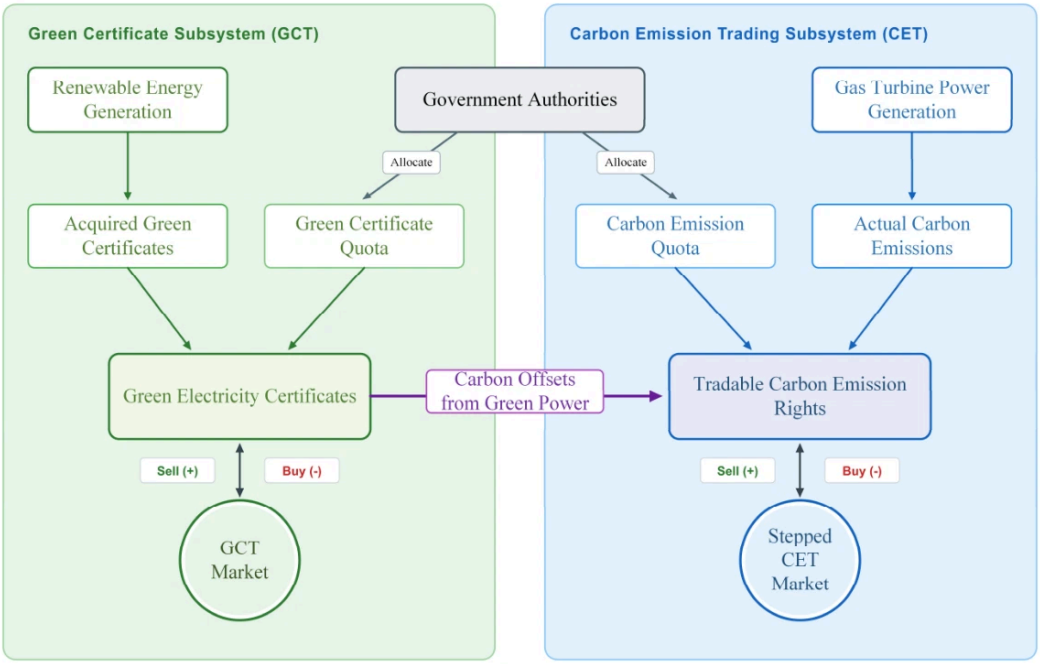

Figure 3. Principle of GCT–CET joint mechanism.

3.3. Stepped Carbon Emission Trading Mechanism

The tiered CET mechanism incorporates a tiered pricing structure to strengthen operational decarbonization flexibility and cost constraints under distinct emission intervals [22]. Specifically, carbon emissions within the RIES stem from two aspects: electricity procurement and the CHP unit, with the purchased power originating from thermal power generation.

$$E_{\mathrm{total}} = \sum_{t=1}^{T} \left(\sigma_{\mathrm{e}} P_{\mathrm{G}}(t) + \sigma_{\mathrm{h}} \left(\sigma_{\mathrm{e,h}} P_{\mathrm{CHP,e}}(t) + P_{\mathrm{CHP,h}}(t)\right)\right) \tag{11}$$

where E_t denotes the total carbon emission quota of the RIES, kg; σ_{e} and σ_{h} represent the carbon emission quotas per unit of generated electrical and thermal power, respectively, kg/(kW·h); $\sigma_{\mathrm{e,h}}$ is the electricity-to-heat conversion factor, kg/(kW·h); $P_{\mathrm{G}}(t)$ is the power purchased from the main grid at time t, kW.

$$\begin{cases} C_{CO_2}(t) = \mu_h \sigma_{e,h} P_{CHP,e}(t) + \mu_h P_{CHP,h}(t) \\ E_{CO_2}(t) = \sum_{t=1}^{T} \left(\mu_e P_G(t) + C_{CO_2}(t) \right) \end{cases} \quad (12)$$

where μ_e and μ_h denote the carbon emission intensities per unit of electrical and thermal load, respectively, kg/(kW·h); $E_{CO_2}(t)$ represents the actual carbon emissions of the system during time period t, kg.

Therefore, the actual carbon emission trading volume E' is:

$$E' = E'_{total} - E_{total} \quad (13)$$

The tiered CET mechanism sets multiple emission intervals with varying unit carbon allowance prices. With the increase in carbon emissions, the unit carbon price escalates accordingly; its mathematical formulation is defined as:

$$F'_{CO2} = \begin{cases} \beta E' & E' \le L \\ \beta(1+\theta)(E'-L) + \beta L & L < E' \le 2L \\ \beta(2+\theta)L + \beta(1+2\theta)(E'-2L) & 2L < E' \le 3L \\ \beta(1+3\theta)(E'-3L) + \beta(3+3\theta)L & 3L < E' \le 4L \\ \beta(1+4\theta)(E'-4L) + \beta(4+6\theta)L & E' > 4L \end{cases} \quad (14)$$

where F'_{CO2} denotes the carbon trading cost under the stepped CET mechanism, CNY; β is the baseline price of carbon trading, CNY/kg; L represents the step interval of carbon emissions, kg; θ is the price escalation rate.

3.4. Joint GCT–CET Trading Mechanism

The coupling of the green certificate trading and stepped carbon emission trading is designed to achieve the low-carbon transition of the RIES through market-based incentive instruments and cost constraints, the principle of which is illustrated in Figure 3.

This multi-dimensional coordinated strategy across source, load, and market domains incentivizes enterprises to proactively curb carbon emissions via price signals. It not only reinforces their intrinsic willingness for emission reduction, but also effectively improves the system's integration capability for volatile renewable energy, thereby serving as an effective pathway to promote the low-carbon transition of the energy system.

The detailed calculation steps for green certificates participating in carbon offsetting are outlined as follows:

(1) Calculation of green certificates participating in carbon offsetting

$$\begin{cases} G_S = G_h - G_n \\ G_S = G_{GCT} + G_m, G_S > 0 \\ F_{GCT} = -\alpha_{GCT} G_S, G_S \le 0 \end{cases} \quad (15)$$

where G_m denotes the green certificates utilized for carbon offsetting, book; F_{GCT} is

the GCT cost of the RIES, CNY; G_S is the difference between the generated green certificates and the quota requirement, book;

(2) Calculation of actual carbon emission trading volume after green certificate participation

$$\begin{cases} \sum_{t=1}^{T} P_m(t) = G_m(\chi_Z)^{-1} \\ E_{green} = \sum_{t=1}^{T} \mu_e P_m(t) \\ E = E' - E_{green} \end{cases} \tag{16}$$

where $P_m(t)$ denotes the electricity volume represented by the green certificates participating in the carbon offset mechanism at time t, kWh; E_{green} represents the carbon emission offset amount, kg.

(3) Calculating joint GCT–CET trading carbon cost

Substituting E calculated from step (2) for E' into (14) yields the stepped CET cost under the joint mechanism, F_{CO2}.

4. Low-Carbon Optimal Scheduling Model of the RIES

This section establishes the RIES optimization model by systematically coordinating the source-side CCP framework, load-side demand response, and market mechanisms. Through rigorous mathematical formulations, the model integrates operational constraints and energy balances to reflect realistic engineering boundaries, enabling the solver to minimize comprehensive costs while maximizing clean energy accommodation.

4.1. Objective Functions

In this paper, the objective function aims to minimize the comprehensive system cost of the RIES, denoted as F, over a dispatch cycle. This cost comprises the energy procurement cost F_{buy}, operation and maintenance cost F_S, IDR compensation cost F_{IDR}, stepped CET cost F_{CO_2}, wind curtailment cost F_{DG}, and GCT cost F_{GCT}, as formulated in (17).

$$F_{min} = F_{buy} + F_S + F_{DG,cut} + F_{GCT} + F_{CO_2} + F_{IDR} \tag{17}$$

(1) energy procurement cost

$$F_{buy} = \sum_{t=1}^{T} (\alpha_t P(t) + \beta_t P_{g,buy}(t)) \tag{18}$$

where $P_{g,buy}(t)$ denotes the purchased natural gas power during time period t, kW; α_t and β_t represent the electricity price and natural gas price at time t, respectively, CNY/(kW·h).

(2) operation and maintenance costs

$$F_S = \sum_{t=1}^{T} \sum_{n} \chi_n P_n(t) \tag{19}$$

where n denotes equipment such as wind power, HGT, ORC, and energy storage; χ_n is the operation and maintenance coefficient of equipment n, CNY/(kW·h); $P_n(t)$ represents the output power of equipment m during time period t, kW.

(3) wind curtailment cost

$$F_{\mathrm{DG,cut}} = \sum_{t=1}^{T} \delta_{\mathrm{DG}} P_{\mathrm{DG,cut}}(t) \tag{20}$$

where δ_{DG} represents the penalty coefficient for wind curtailment during time period t, CNY/(kW·h); $P_{\mathrm{DG,cut}}(t)$ denotes the curtailed wind power at time t, kW.

(4) The GCT cost is detailed in (10).

(5) The stepped CET cost is formulated in (14)–(16).

(6) IDR compensation cost

$$F_{\mathrm{IDR}} = \sum_{i=1}^{3} \sum_{t=1}^{T} \left(C_{\mathrm{P}} \left| \Delta P_{i,\mathrm{L}}^{\mathrm{P}}(t) \right| + C_{\mathrm{K}} \left| \Delta P_{i,\mathrm{L}}^{\mathrm{K}}(t) \right| \right) \tag{21}$$

where C_{P} and C_{K} denote the unit compensation coefficients for shiftable loads and substitutable loads participating in demand response, respectively, in CNY/kW.

(7) Total revenue function

$$R_{\mathrm{total}} = \sum_{t=1}^{T} \left(P_{\mathrm{e,sell}}(t) C_{\mathrm{sell,e}}(t) + P_{\mathrm{h,sell}}(t) C_{\mathrm{sell,h}}(t) + P_{\mathrm{g,sell}}(t) C_{\mathrm{sell,g}}(t) \right) + R_{\mathrm{GCT}} \tag{22}$$

where R_{total} is the total revenue; $P_{\mathrm{e,sell}}(t)$, $P_{\mathrm{h,sell}}(t)$, and $P_{\mathrm{g,sell}}(t)$ denote the selling powers of electricity, heat, and gas, respectively, and $C_{\mathrm{sell,e}}(t)$, $C_{\mathrm{sell,h}}(t)$, and $C_{\mathrm{sell,g}}(t)$ represent the selling prices of electricity, heat, and gas, respectively.

4.2. Constraints

(1) Wind Power Output Constraints

$$\begin{cases} P_{\mathrm{wind}}^{\max} = P_{\mathrm{wind}}(t) + P_{\mathrm{DG}}(t) \\ 0 \le P_{\mathrm{wind}}(t) \le P_{\mathrm{wind}}^{\max} \\ 0 \le P_{\mathrm{DG}}(t) \end{cases} \tag{23}$$

where $P_{\mathrm{wind}}^{\max}$ denotes the upper bound of wind power generation, kW. $P_{\mathrm{DG}}(t)$ represents the curtailed wind power.

(2) HFC Operational Constraints

$$\begin{cases} P_{\mathrm{HFC,e}}(t) = \eta_{\mathrm{HFC,e}} P_{\mathrm{HFC}}^{\mathrm{H}}(t) \\ P_{\mathrm{HFC,h}}(t) = \eta_{\mathrm{HFC,h}} P_{\mathrm{HFC}}^{\mathrm{H}}(t) \\ P_{\mathrm{HFC}}^{\mathrm{H,min}} \le P_{\mathrm{HFC}}^{\mathrm{H}}(t) \le P_{\mathrm{HFC}}^{\mathrm{H,max}} \\ \Delta P_{\mathrm{HFC}}^{\mathrm{H,min}} \le P_{\mathrm{HFC}}^{\mathrm{H}}(t+1) - P_{\mathrm{HFC}}^{\mathrm{H}}(t) \le \Delta P_{\mathrm{HFC}}^{\mathrm{H,max}} \end{cases} \tag{24}$$

where $P_{\mathrm{HFC}}^{\mathrm{H}}(t)$ represents the hydrogen power input to the HFC at time t, kW; $P_{\mathrm{HFC,e}}(t)$ and $P_{\mathrm{HFC,h}}(t)$ are the electrical and thermal power outputs of the HFC at time t, respectively, kW; $P_{\mathrm{HFC}}^{\mathrm{H,max}}$ and $P_{\mathrm{HFC}}^{\mathrm{H,min}}$ are the upper and lower limits of the hydrogen power input to the HFC, respectively, kW; $\eta_{\mathrm{HFC,h}}$ and $\eta_{\mathrm{HFC,e}}$ denote the thermal and electrical conversion efficiencies of the HFC, respectively; $\Delta P_{\mathrm{HFC}}^{\mathrm{H,max}}$ and $\Delta P_{\mathrm{HFC}}^{\mathrm{H,min}}$ represent the upper and lower ramp rate limits of the HFC, respectively, kW.

(3) CCP Coupled Operational Constraints

$$\begin{cases} P_{\mathrm{e,EL}}^{\min} \le P_{\mathrm{e,EL}}(t) \le P_{\mathrm{e,EL}}^{\max} \\ P_{\mathrm{H,MR}}^{\min} \le P_{\mathrm{H,MR}}(t) \le P_{\mathrm{H,MR}}^{\max} \\ 0 \le P_{\mathrm{CCS}}(t) \le P_{\mathrm{CCS}}^{\max} \end{cases} \tag{25}$$

where $P_{\mathrm{e,EL}}^{\max}$ and $P_{\mathrm{e,EL}}^{\min}$ denote the upper and lower limits of the energy consumption of the EL during time period t, respectively, kW; $P_{\mathrm{H,MR}}^{\max}$ and $P_{\mathrm{H,MR}}^{\min}$ represent the upper and lower bounds of the hydrogen power input to the MR, respectively, kW; $P_{\mathrm{CCS}}^{\max}$ is the maximum operational power of the CCS, kW; ε is an infinite decimal.

(4) Energy Storage Constraints

$$\begin{cases} E_i(t) = E_i(t-1) + \left(P_{\mathrm{ES,in}}^{i}(t)\gamma_{i,\mathrm{in}} - \dfrac{P_{\mathrm{ES,out}}^{i}(t)}{\gamma_{i,\mathrm{out}}}\right)\Delta(t) \\ E_i(1) = E_i(T) = 0.5E_{i,\max} \\ E_{i,\min} \le E_i(t) \le E_{i,\max} \\ r_{\mathrm{ES,in}}^{i}(t) + r_{\mathrm{ES,out}}^{i}(t) = 1 \\ 0 \le P_{\mathrm{ES,in}}^{i}(t) \le r_{\mathrm{ES,in}}^{i}(t) P_{\mathrm{ES,in}}^{i,\max} \\ 0 \le P_{\mathrm{ES,out}}^{i}(t) \le r_{\mathrm{ES,out}}^{i}(t) P_{\mathrm{ES,out}}^{i,\max} \end{cases} \tag{26}$$

where $P_{\mathrm{ES,in}}^{i}(t)$ and $P_{\mathrm{ES,out}}^{i}(t)$ represent the charging and discharging powers of the i-th type of energy storage at time t, respectively, kW; i denotes the energy type, including electricity, heat, gas, and hydrogen; $E_i(t)$ is the stored energy of the i-th type of energy storage at time t, kWh; $\gamma_{i,\mathrm{in}}$ and $\gamma_{i,\mathrm{out}}$ are the charging and discharging efficiencies of the i-th type of energy storage, respectively; $E_{i,\max}$ and $E_{i,\min}$ denote the upper and lower capacity limits of the i-th type of energy storage, respec-

tively, kWh; $r^{i}_{\mathrm{ES,in}}(t)$ and $r^{i}_{\mathrm{ES,out}}(t)$ are the state variables of the i type of energy storage; $P^{i,\max}_{\mathrm{ES,in}}$ and $P^{i,\max}_{\mathrm{ES,out}}$ denote the highest storage and release power of the i category of energy storage. $\Delta(t)$ is 1 h.

4.3. Energy Balance Constraints

In this paper, the electricity, heat, gas, and hydrogen energy balance constraints of the RIES are as follows:

$$\begin{cases} P_{\mathrm{wind}}(t)+P_{\mathrm{HFC,e}}(t)+P_{\mathrm{CHP,e}}(t)+P^{\mathrm{e}}_{\mathrm{ES,dis}}(t)=P_{\mathrm{e,load}}(t)+P^{\mathrm{e}}_{\mathrm{ES,chr}}(t)-P_{\mathrm{G}}(t) \\ P_{\mathrm{CHP,h}}(t)+P_{\mathrm{HFC,h}}(t)+P^{\mathrm{h}}_{\mathrm{ES,dis}}(t)=P_{\mathrm{h,load}}(t)+P^{\mathrm{h}}_{\mathrm{ES,chr}}(t) \\ P_{\mathrm{g,buy}}(t)+P_{\mathrm{MR,CH_4}}(t)+P^{\mathrm{g}}_{\mathrm{ES,dis}}(t)=P_{\mathrm{g,load}}(t)+P_{\mathrm{CH_4,GT}}(t)+P^{\mathrm{g}}_{\mathrm{ES,chr}}(t) \\ P_{\mathrm{EL,H}}(t)+P^{\mathrm{H}}_{\mathrm{ES,dis}}(t)=P_{\mathrm{H,MR}}(t)+P_{\mathrm{H,HFC}}(t)+P_{\mathrm{H,GT}}(t)+P^{\mathrm{H}}_{\mathrm{ES,chr}}(t) \end{cases} \quad (27)$$

where $P^{\mathrm{h}}_{\mathrm{ES,chr}}(t)$ and $P^{\mathrm{h}}_{\mathrm{ES,dis}}(t)$ represent the charging and discharging powers of the battery during time period t, respectively, kW; $P^{\mathrm{g}}_{\mathrm{ES,chr}}(t)$ and $P^{\mathrm{g}}_{\mathrm{ES,dis}}(t)$ denote the gas injection and withdrawal powers of the gas storage tank at time t, respectively, kW; $P^{\mathrm{H}}_{\mathrm{ES,chr}}(t)$ and $P^{\mathrm{H}}_{\mathrm{ES,dis}}(t)$ are the hydrogen injection and withdrawal powers of the hydrogen storage tank at time t, respectively, kW.

4.4. Model Solution

The problem investigated in this study is formulated as a mixed-integer linear programming model. To effectively coordinate the bidirectional interaction between the source-side CCP coupling model and the load-side IDR, a joint green-certificate trading and stepped carbon-emission trading mechanism is introduced. On this basis, a low-carbon optimal dispatch model for the RIES is established within the electricity market framework considering source–load interaction. With the objective of minimizing the total system operating cost, the formulated model is solved under multiple operational constraints via the YALMIP toolbox with the CPLEX solver in MATLAB, thereby determining the optimal dispatch schedule.

The overall scheduling workflow of the model is illustrated in Figure 4. Figure 4 demonstrates the entire process ranging from source-side unit scheduling, electricity price signal generation, and load-side response to source-side feedback adjustment, reflecting the structural feedback closed-loop mechanism formed between the source and the load under the coordination of the centralized optimizer.

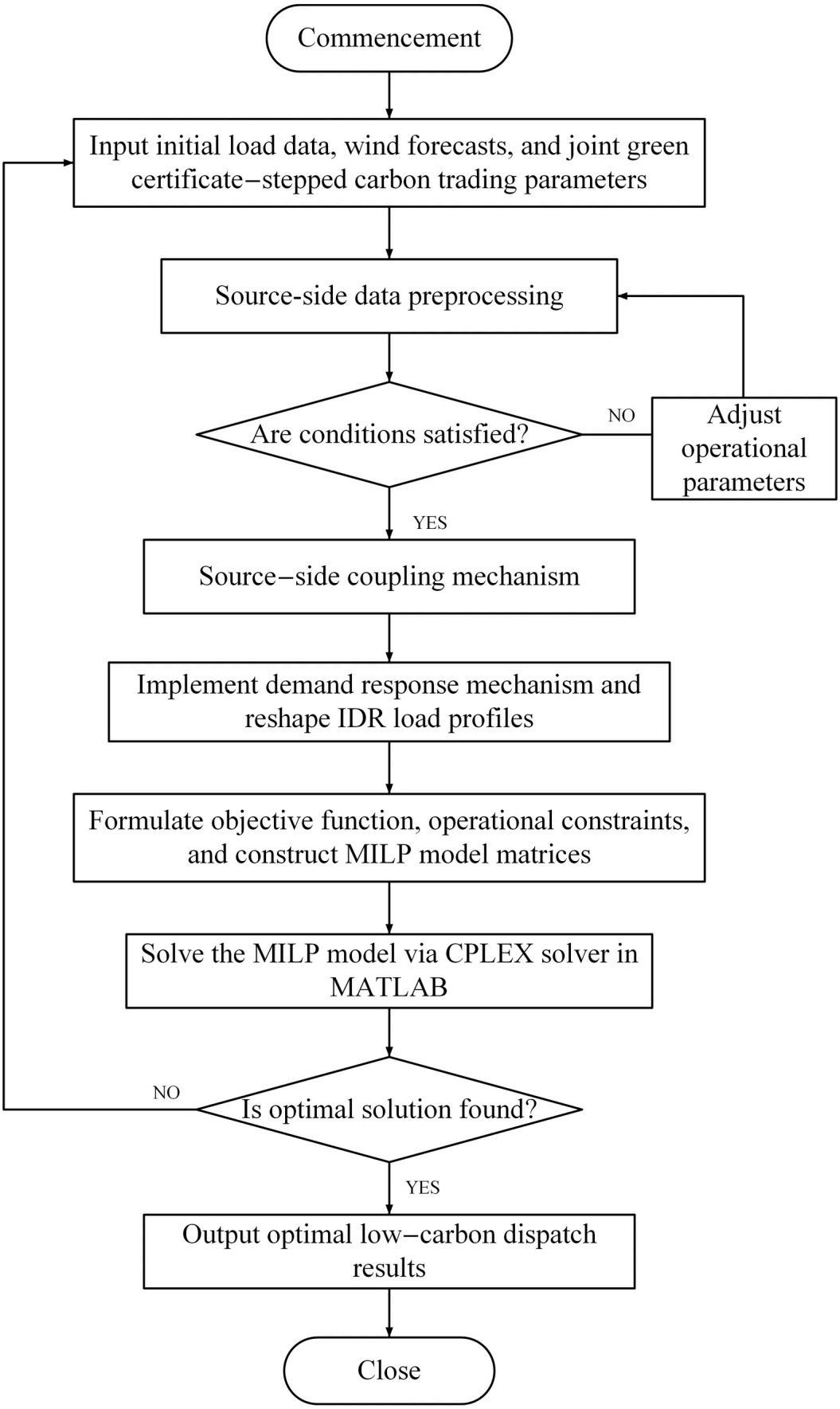

Figure 4. Source–Load Coordinated Dispatch Procedure.

5. Case Study

This section validates the effectiveness and superiority of the proposed low-carbon optimal scheduling strategy for the regional integrated energy system through case studies. By establishing multiple comparative operational scenarios, the effectiveness of the source-side CCP coupling, load-side IDR, and the GCT-CET joint market mechanism is verified. In addition, sensitivity analyses regarding key market prices are conducted to provide deeper managerial insights. The simulation results provide solid evidence of the strategy's capability in promoting renewable energy accommodation and reducing carbon emissions.

5.1. System Parameters and Scenario Settings

In this paper, a regional integrated energy system (RIES) park is selected as a case study [23], and a 24-h scheduling horizon is adopted to verify and analyze the proposed low-carbon RIES dispatch model across various operating scenarios. Figure 5 presents the forecasted wind power output and load profiles of the RIES. Additionally, the parameters of the energy storage systems and coupling devices are itemized in Tables 1 and 2, respectively. Table 3 lists the time-of-use electricity and gas prices, Table 4 specifies the configurations of the operating scenarios, and the data regarding the green certificate and carbon trading markets are referenced in reference [24].

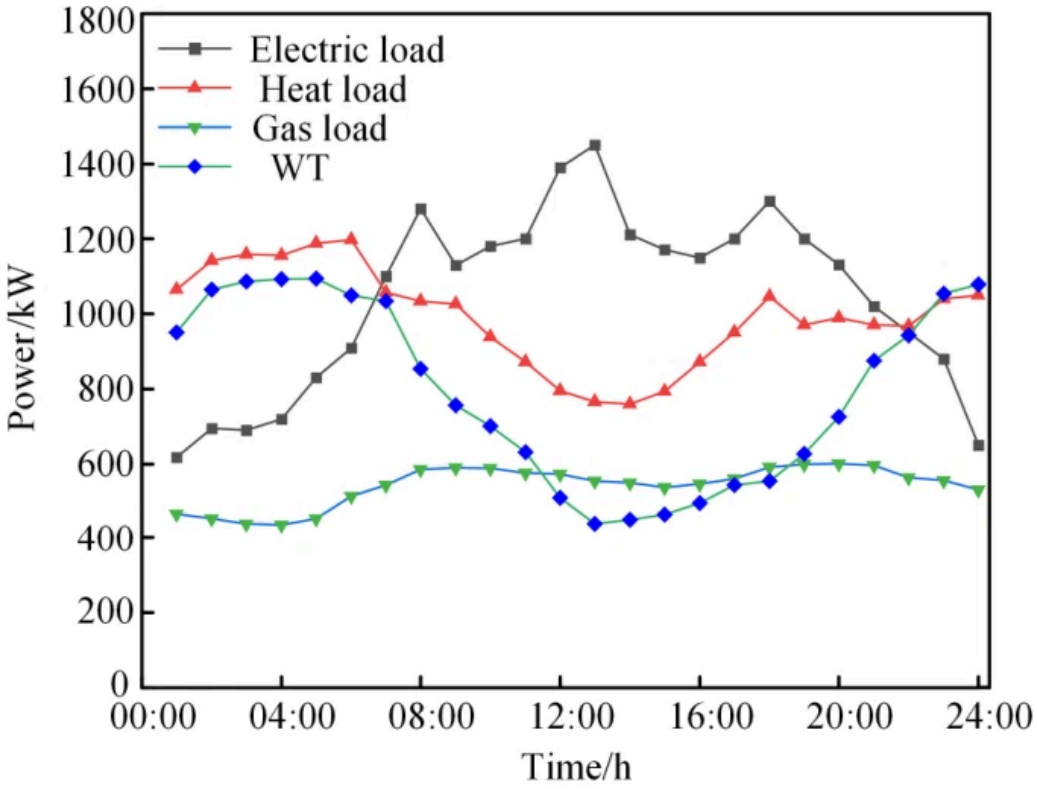

Figure 5. Forecast Curves for Wind Power Generation and Load Consumption.

Table 1. Parameters of energy storage device.

Equipment	Capacity (kW)	Storage Capacity Upper and Lower Limits (%)	Charging and Discharging Efficiency (%)	Ramp Constraint (%)	Maintenance Cost (CNY/kWh)
EES	450	90, 10	95	20	0.021

Equipment	Capacity (kW)	Storage Capacity Upper and Lower Limits (%)	Charging and Discharging Efficiency (%)	Ramp Constraint (%)	Maintenance Cost (CNY/kWh)
TES	500	90, 10	95	20	0.016
GES	300	90, 10	95	20	0.018
HES	300	90, 10	95	20	0.020

Table 2. Equipment parameters of RIES.

Equipment	Capacity (kW)	Conversion Efficiency (%)	Maintenance Cost (CNY/kWh)
HGT	800	Electricity: 40 Heat: 55	0.030
EB	500	80	0.020
WHB	500	85	0.023
ORC	500	20	0.050
EL	500	87	0.040
MR	350	65	0.030
HFC	300	Electricity:40 Heat: 55	0.035
CCS	600	90	0.045

Table 3. Energy purchase price.

Time Period	Electricity Price (CNY/kWh)	Gas Price (CNY/kWh)
01:00—07:00 22:00—24:00	0.48	0.45
07:00—11:00 14:00—18:00	0.67	0.36
11:00—14:00 18:00—22:00	1.2	0.25

Table 4. Comparative Analysis of Different Operation Scenarios.

Scenario	Carbon Trading	Source-Side Flexibility Retrofitting	IDR
1	Traditional	Traditional P2G and CHP	Not considered
2	Traditional	Two-stage P2G combined with HFC operation	Not considered
3	Traditional	Add CCS equipment, construct CCP coupling model	Not considered
4	Traditional	Same as Scenario 3	Considered
5	Joint GCT-CET mechanism	Same as Scenario 3	Not considered

Scenario	Carbon Trading	Source-Side Flexibility Retrofitting	IDR
6	Joint GCT-CET mechanism	Same as Scenario 3	Considered

5.2. Results and Discussion

5.2.1. Comparative Analysis of Scenario Results

The optimization scheduling results for the aforementioned scenarios are presented in Table 5.

Table 5. Comparison of scene results.

Scenario	Total Cost (CNY)	Total Revenue (CNY)	Total Profit (CNY)	Carbon Emissions (kg)	Maintenance Cost (CNY)	CET Cost (CNY)	GCT Cost (CNY)	IDRCost (CNY)	Wind Power Utilization Rate (%)
1	32,512	58,503	25,991	25,763	2537	1035	0	0	56.17
2	30,134	58,964	28,830	22,479	2830	851	0	0	68.34
3	28,961	60,113	31,152	20,137	3319	632	0	0	72.16
4	26,873	61,357	34,484	18,361	3548	580	0	2215	77.35
5	24,539	62,578	38,039	16,870	3617	556	2731	0	86.38
6	21,748	61,318	39,570	15,534	3795	552	2438	2536	92.74

(1) From the perspective of economic performance, a comparison among Scenarios 1, 2, and 3 reveals that the total cost of Scenario 3 (CNY 28,961) is lower than that of Scenarios 1 and 2 by CNY 3551 and CNY 1173, respectively. Due to the integration of CCS equipment, the operation and maintenance cost in Scenario 3 increases by CNY 782 and CNY 489 compared to Scenarios 1 and 2, respectively. Meanwhile, the total profit of CNY 31,152 in Scenario 3 increases by CNY 5161 and CNY 2322 relative to Scenarios 1 and 2. This indicates that the proposed coupling model effectively reduces external energy procurement demand by supplying CO_2 captured by CCS to the methanation reaction, thereby promoting wind power accommodation and carbon emission reduction. Although the increased equipment complexity leads to higher maintenance costs, the overall system operating cost still exhibits a downward trend.

From the perspectives of carbon emissions and wind power accommodation, Scenario 3 achieves a carbon emission level of 20,137 kg, which represents reductions of 5626 kg and 2342 kg compared to Scenarios 1 and 2, respectively. Furthermore, its wind power utilization rates increase by 15.99 and 3.82 percentage points, respectively. These results demonstrate that the proposed coupling model allows the system to operate P2G at higher power levels during periods of wind generation by utilizing CO2 captured via MR, thereby achieving a synergistic enhancement of both low-carbon performance and renewable energy accommodation capability.

(2) In Scenario 4, after incorporating IDR, the total system cost decreases to CNY 26,873 compared to Scenario 3, with carbon emissions reduced by 1776 kg and the wind power accommodation rate increased to 77.35%. This is because the load-side response timing matches the source-side output, shifting peak-period loads to low-price periods and thereby alleviating source-side peak-shaving pressure. When the joint GCT-CET trading mechanism is introduced in Scenario 6, the total system cost decreases by CNY 5125, carbon emissions are reduced by 2827 kg, and the wind power accommodation

rate rises to 92.74%. These results demonstrate that the joint mechanism incentivizes the system to proactively accommodate wind power through green certificate revenues and carbon pricing signals; although it incurs a joint trading cost of CNY 2960, the overall profit increases by CNY 5086, reflecting the economic effectiveness of the joint GCT-CET mechanism in reinforcing source–load interaction. In Scenario 5, replacing the IDR of Scenario 4 with the joint GCT-CET mechanism significantly reduces carbon emissions, improves the efficient utilization of source-side energy, and increases the wind power accommodation rate to 86.38%. Scenario 6 comprehensively accounts for the source-side CCP coupling model and the load-side IDR model while incorporating the joint GCT-CET mechanism, thereby establishing a source–load interactive cooperative optimization mechanism based on the electricity market. Specifically, the source-side enhances flexible regulation and the capacity to absorb surplus power, while the load-side relies on market mechanisms to align demand response with system operation objectives, ultimately achieving a peak wind power accommodation rate of 92.74%.

5.2.2. Operation Analysis of the CCP Coupling Model

As illustrated in Figure 6, Scenario 1 considers traditional P2G. Although it can accommodate a portion of wind power by converting it into natural gas, significant wind curtailment still exists due to limitations in equipment regulation ranges and overall energy efficiency. In Scenario 2, EL and MR are utilized to replace traditional P2G and operate in conjunction with HFC. The hydrogen generated by EL exhibits greater flexibility; it can not only be combined with CO_2 via MR to synthesize methane and reduce system energy procurement costs, but can also be supplied to HFC for efficient CHP generation. Compared with Scenario 1, this electricity–hydrogen multi-energy conversion pathway broadens the space for wind power accommodation, yet its unstable carbon sources increase the system energy procurement costs. Scenario 3 significantly reduces system carbon emissions by incorporating CCS to construct a deep CCP coupling model. This model captures CO_2 emitted from CHP units via CCS to serve as a stable carbon source for the methanation reaction, thereby achieving a complete closed-loop of carbon elements within the system from emission and capture to energetic utilization. Compared with Scenario 2, it reduces carbon emissions and energy procurement costs. Although the operation and maintenance costs increase, the overall operating economic efficiency and low-carbon performance of the system are significantly enhanced.

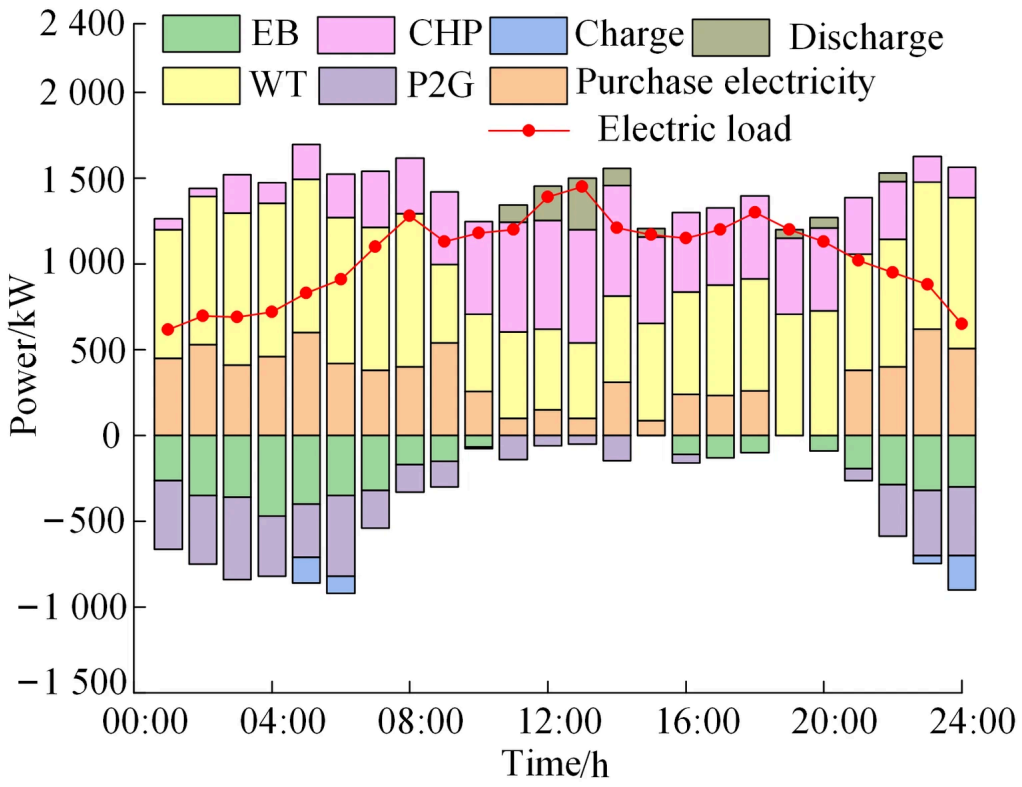

(a)

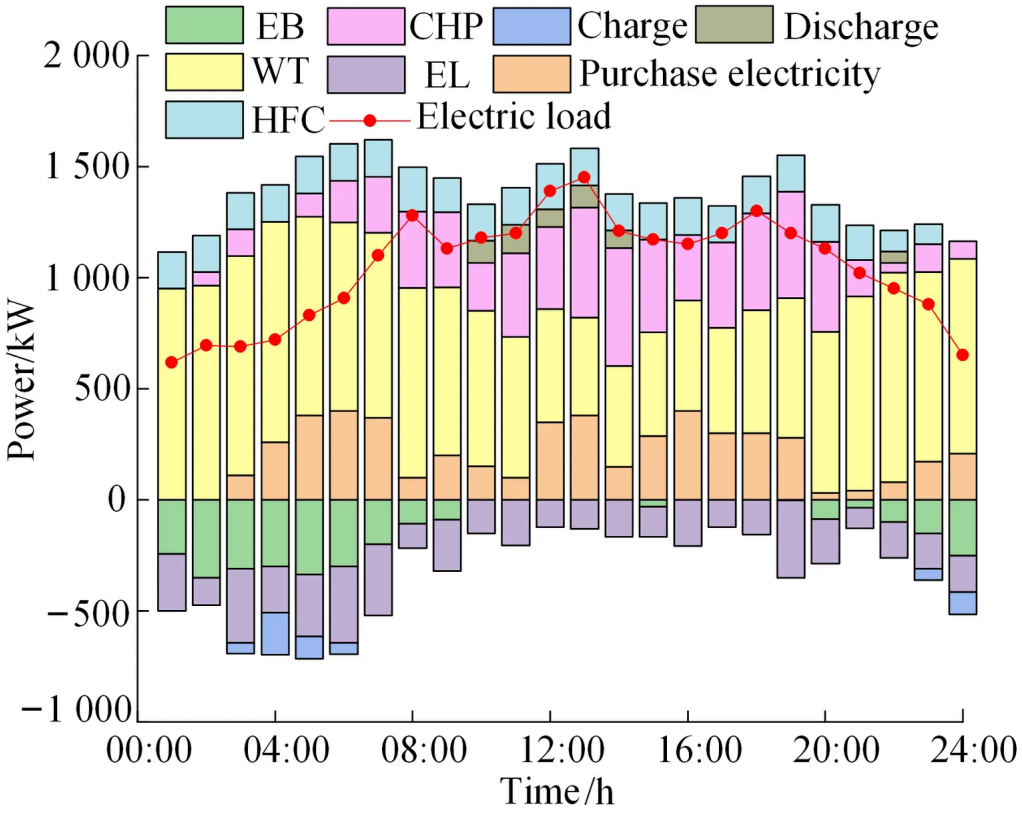

(b)

https://doi.org/10.3390/en19235776

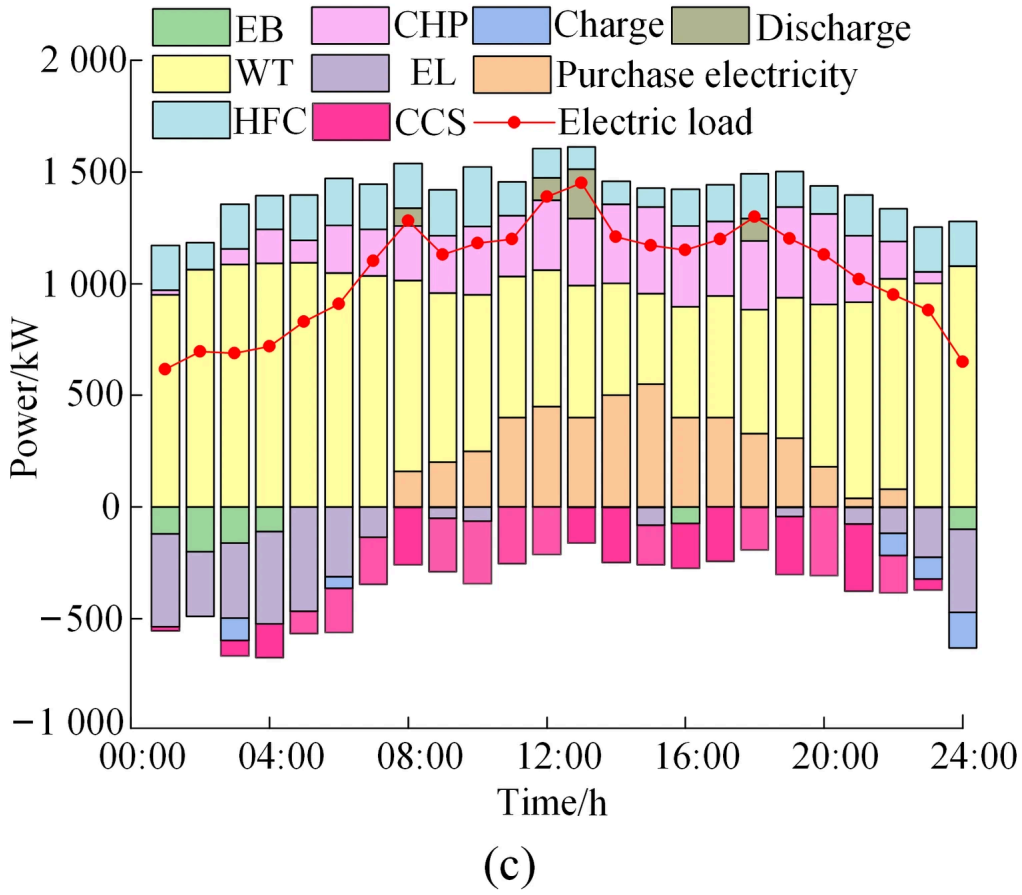

Figure 6. Electrical power balance diagrams: (**a**) Scenario 1; (**b**) Scenario 2; (**c**) Scenario 3.

5.2.3. Impacts of the Joint GCT-CET Mechanism and IDR Cooperative Optimization on RIES

Figures 7 and 8 show the comparison of electrical and thermal load curves before and after considering the IDR model, as well as the corresponding EL output for Scenarios 3, 5, and 6, respectively.

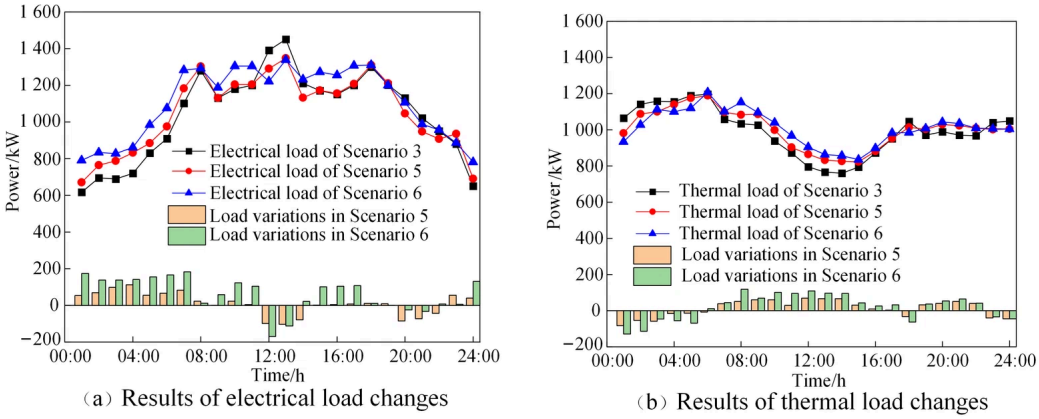

Figure 7. Comparison of Load Variation Results.

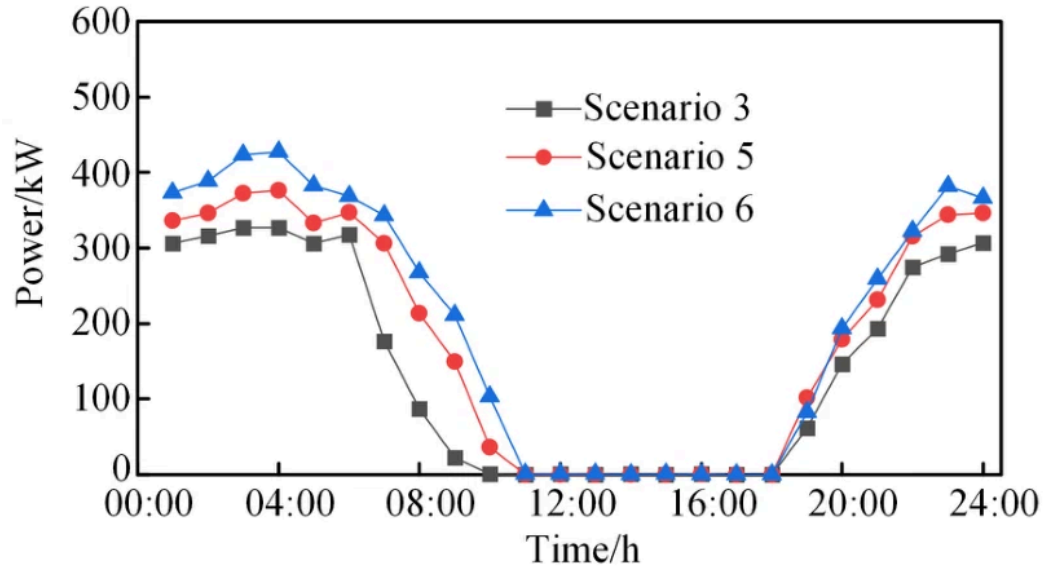

Figure 8. Electrolyzer output in scenarios 3, 5, 6.

As shown in Figure 7a, the electrical load is shifted out during the peak-price periods of 10:00–13:00 and 18:00–22:00. During these periods, natural gas prices remain at a relatively low level; thus, through load substitution, a portion of the electrical load is replaced by thermal and gas loads, thereby achieving "peak shaving" on the electricity side. During the periods of high wind power output and low electricity prices from 01:00–07:00 and 22:00–24:00, the electrical load is shifted via inter-temporal translation to replace part of the thermal and gas loads, achieving a "valley filling" effect. Consequently, the maximum peak-to-valley difference decreases from 833 kW to 570 kW, representing a reduction of 31.57%. This indicates that the time-of-use electricity price signal can effectively optimize the load distribution, thereby reducing the peak-to-valley difference of the load curve.

As shown in Figure 7b, the thermal load is shifted out during the peak period of 01:00–07:00. At this time, the system prioritizes the use of wind power to drive EL for hydrogen production, which is then converted into thermal and electrical energy via HFC equipment, thereby reducing system electricity procurement and accommodating a large amount of wind power. The thermal load is shifted in during the valley period of 13:00–17:00, utilizing the substitution of electrical and gas loads to effectively flatten the valley, reducing the maximum peak-to-valley difference from 432 kW to 341 kW, a reduction of 21.06%. Through the cross-substitution and cooperative complementarity of multiple energies, the fluctuations in the load curve are smoothed out. The connection between the load-side and source-side equipment is established through the joint mechanism, which leverages incentives to alter energy-consumption behavior, lower costs, enhance the wind power accommodation rate, and achieve a dynamic balance between wind power accommodation and low-carbon operation costs.

As can be seen from Figures 7 and 8 and Table 5, under the synergistic effect of the joint GCT-CET mechanism and IDR, Scenario 6 achieves a 14.59% reduction in system cost and a 5.2% reduction in carbon emissions compared to Scenario 5. By enhancing the wind power utilization rate and EL hydrogen production during low-load periods, as well as the flexible conversion of hydrogen energy, electricity procurement during peak load hours is reduced, leading to a significant decrease in the peak-to-valley difference of the system load curve. Although the IDR subsidy cost increases, the comprehensive cost is significantly reduced, which verifies the effectiveness of cooperative optimization in simultaneously balancing system economics, regulation flexibility, and low-carbon en-

vironmental protection.

5.2.4. Impacts of the Base Prices of the GCT-CET Mechanism on System Operation

To investigate the impacts of the base prices of the two mechanisms on wind power utilization, carbon emissions, and total costs under this joint market mechanism, comparative analyses were conducted based on Scenario 6 under various green certificate and carbon trading prices, as illustrated in Figure 9.

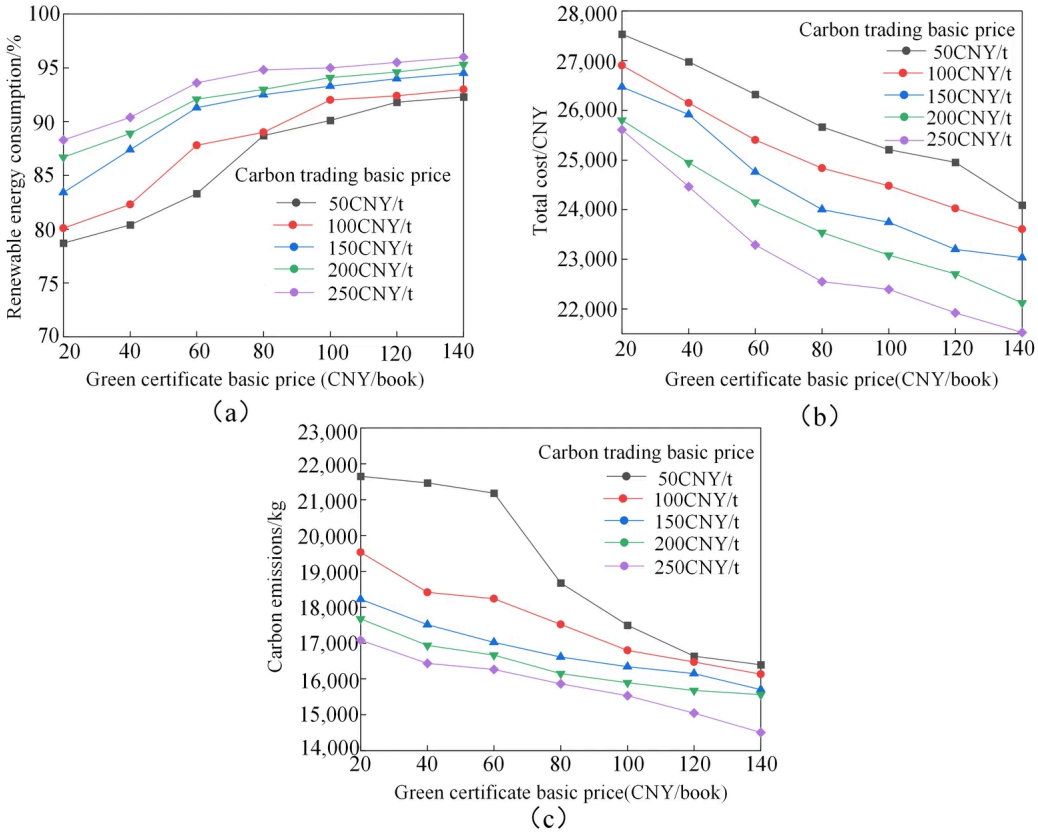

Figure 9. Simulation results: (**a**) Renewable energy consumption rate under different prices; (**b**) variations in total system cost; (**c**) carbon emissions under different prices.

As can be seen from Figure 9a–c, when the mechanism prices are low, the system exhibits weak sensitivity to these mechanisms; as the prices rise, their impact on the system gradually becomes significant. Increasing the base price of green certificates can effectively enhance wind power revenue and subsequently improve the wind accommodation level, while increasing the baseline price of carbon trading helps constrain system carbon emissions. However, relying solely on the price regulation of a single mechanism makes it difficult to simultaneously balance wind power accommodation and low carbon emissions. This indicates that reasonably setting the prices in the joint market can effectively increase the wind power accommodation rate and reduce carbon emissions.

As illustrated in Figure 9b, with the increase in prices, the impacts of both mechanisms are enhanced, and the total cost of the system exhibits a clear downward trend. This is because the increases in the baseline prices of green certificates and carbon trading prompt the system to prioritize wind power accommodation and reduce carbon emissions, thereby boosting revenues from the GCT and stepped CET, which in turn drive down the total cost. Therefore, to control the carbon emissions and total cost of the RIES, greater emphasis should be placed on setting the baseline prices for carbon trading

and green certificates, as reasonable pricing can achieve the low-carbon and economic operation of the system.

5.2.5. Quantitative Analysis of GCT-CET Mechanism and Load-Side Coordination

To quantify the incremental benefits of market mechanisms and load-side coordinated dispatch, based on Scenarios 4, 5, and 6, this paper introduces two relative indicators: the joint economic advantage (JEA) and the joint carbon advantage (JCA). These indicators are used to evaluate the advantages of cost reduction and carbon mitigation under joint dispatch compared to any single mechanism, and the visualization results are illustrated in Figure 10.

$$\begin{cases} \lambda_{\mathrm{JEA}} = \dfrac{E_{\mathrm{a}} - E_{\mathrm{b}}}{E_{\mathrm{a}}} \times 100\,\% \\ \lambda_{\mathrm{JCA}} = \dfrac{C_{\mathrm{a}} - C_{\mathrm{b}}}{C_{\mathrm{a}}} \times 100\,\% \end{cases} \tag{28}$$

where E_{a} is the system cost under a single mechanism; E_{b} is the system cost under the joint mechanism; C_{a} is the carbon emissions under a single mechanism; and C_{b} is the carbon emissions under the joint mechanism.

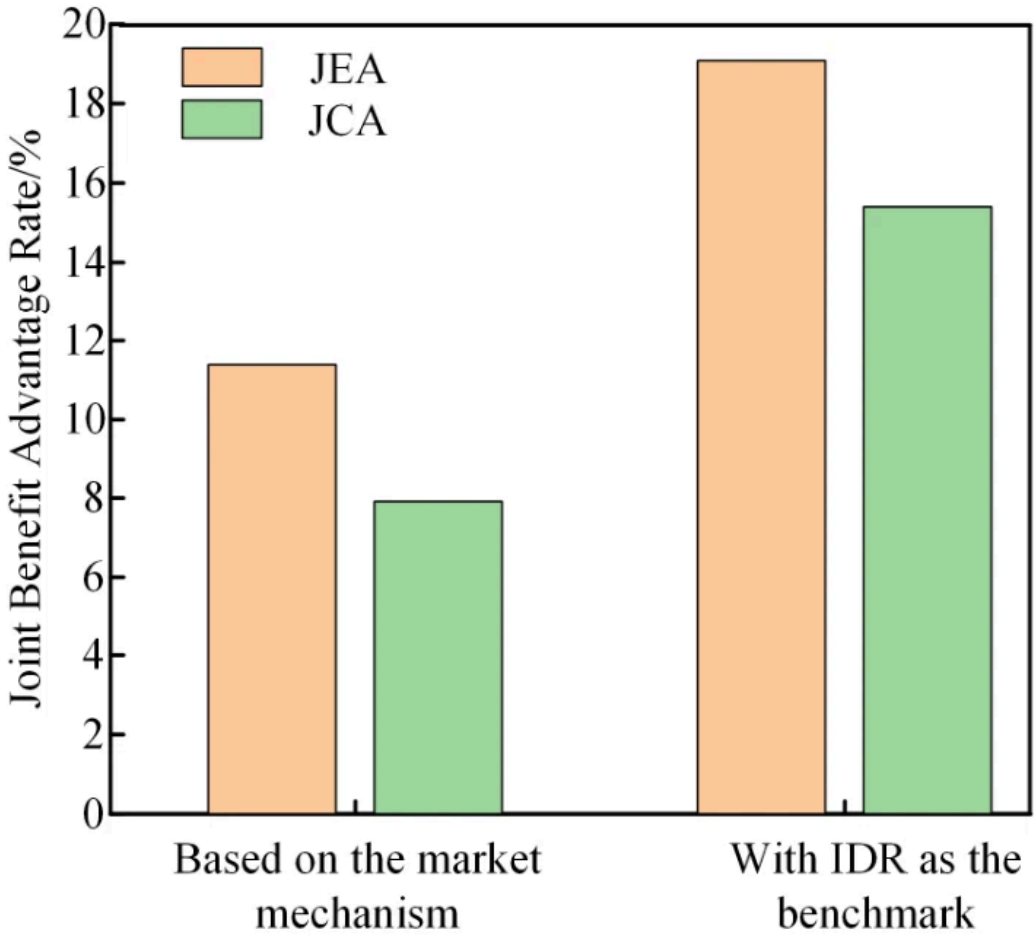

Figure 10. Comparison of synergy gains between single and dual mechanisms.

As can be seen from Figure 10, taking the market mechanism as the benchmark, coordinated dispatch reduces the operating cost by 11.37% and carbon emissions by 7.92%; taking the IDR as the benchmark, the operating cost decreases by 19.07% and carbon emissions decrease by 15.4%. The results demonstrate that, compared with a single

mechanism, the dual mechanism exhibits significant advantages in enhancing the low-carbon economic performance of the system.

The source-side mechanism achieves direct emission reductions through the carbon capture and power coupling model, albeit with an increase in operating costs. When considering load demand, load shifting and substitution effectively reduce peak energy purchase demands and alleviate source-side peak-regulation pressure. Although the load-side mechanism can improve load timing profiles, its emission reduction capacity is limited, whereas the incorporation of the source-side mechanism compensates for its shortcomings in carbon control. The two mechanisms complement each other in scheduling functions, achieving bidirectional optimization through source–load synergy and significantly enhancing the overall operational performance of the regional integrated energy system.

6. Conclusions

(1) The coordinated operation of Power-to-Gas and Carbon Capture and Storage on the source side, through the recycling of carbon elements, establishes a Carbon Capture and Power-to-Gas coupling model. This model creates a closed-loop path for carbon capture, conversion, and reuse within the system, resulting in a 10.92% reduction in the total operating cost of the integrated energy system and a 21.84% decrease in carbon emissions. This validates the effectiveness of carbon cycling in enhancing the coupling efficiency of multi-energy flows.

(2) The introduction of the joint Green Certificate Trading and Carbon Emission Trading mechanism effectively guides the coordination between load-side resource regulation and source-side CCP units via market signals. Through multi-energy complementarity and inter-temporal shifting on the load side in conjunction with source-side equipment operation, the mechanism not only reduces the peak-to-valley difference in the net load but also increases the wind power accommodation rate. Furthermore, a quantitative analysis comparing the incremental benefits of the GCT-CET mechanism and load-side coordination is presented.

(3) Sensitivity analysis demonstrates that reasonable parameter settings are conducive to maximizing the effectiveness of the joint GCT-CET mechanism and improving the low-carbon economic performance of the system. However, control of carbon emission levels does not rely solely on this joint mechanism; instead, the source–load dispatch strategy is dynamically adjusted according to market fluctuations and system operating states to achieve the co-optimization of economic operation and low-carbon emission reduction.

The model established in this paper may not fully capture the complexity of real-world applications, and factors such as market fluctuations and user behavior variations may affect the practical effectiveness of the proposed model. Future work will investigate the impacts of source–load uncertainties and user comfort constraints on scheduling strategies, while validating the effectiveness of the scheduling strategies under user comfort requirements across different seasons.

Author Contributions: Validation, P.C.; writing—original draft, P.C.; writing—review & editing, J.D.; supervision, J.D. All authors have read and agreed to the published version of the manuscript.

Funding: This research was funded by the National Natural Science Foundation of China (NSFC), grant number National Natural Science Foundation Project (61703144).

Data Availability Statement: The meteorological data, parameter settings, and MATLAB/YALMIP scheduling code generated and analyzed during the current study are available from the corresponding author upon reasonable request.

Conflicts of Interest: The authors declare no conflicts of interest.

Nomenclature

Abbreviations		P	Power
CHP	Combined heat and power	τ_{HGT}	Hydrogen-blending volumetric ratio in HGT
CCS	Carbon capture and storage	L^{V}	Gas heating value
P2G	Power to gas	Q_{n}	Green certificate quota
CCP	CHP-CCS-P2G	Q_{h}	Green certificate volume
ORC	Organic Rankine cycle	Q_{GCT}	Volume of green certificates participating in market trading
EB	Electric boiler	α_{GCT}	Unit price of green certificates
GCT	Green certificate trading	χ	Green certificate quota coefficient
CET	Carbon emission trading	μ	Carbon emission intensity
MR	Methane reactor	σ	Emission intensity per unit power
EL	Electrolyzer	β	Base price of carbon emission trading
HGT	Hydrogen-blended gas turbine	L	Carbon emission tier interval length
IDR	Integrated demand response	θ	Price growth rate for stepped carbon trading
HFC	Hydrogen fuel cell	Q_{S}	Remaining green certificates
RIES	Regional integrated energy systems	Q_{m}	Certificates participating in carbon offset
WT	Wind turbine	δ_{DG}	Penalty coefficient for wind power curtailment
WHB	Waste heat boilers	χ_{m}	Operation and maintenance cost coefficient

EES	Electrical energy storage	C	Compensation coefficient
TES	Thermal energy storage	P_{ES}^{i}	Energy storage type
GES	Gas energy storage	γ	Energy storage charge and discharge
HES	Hydrogen energy storage	e	Electrical
JEA	Joint economic advantage	H	Hydrogen
JCA	Joint carbon advantage	h	Thermal
Parameters		g	Gas
η	Energy conversion efficiency	i	Load category
λ_{e}	Energy consumption per unit of captured CO_2	S	Fixed load
α_t	Electricity purchase price	P	Transferable load
β_t	Gas price	K	Substitutable load
ΔP	Power variation	max	Maximum
t	Within a certain period	min	Minimum
T	Scheduling time horizon	in	Input Power
$\sigma_{e,h}$	Electrical-to-thermal conversion coefficient	out	Output Power
β_{EB}	EB electricity-to-heat conversion coefficient	k	Status variable

References

1. IPCC. *Special Report on Global Warming of 1.5 °C*; Cambridge University Press: Cambridge, UK, 2018. [Google Scholar]
2. Hanif, I.; Aziz, B.; Chaudhry, I.S. Carbon emissions across the spectrum of renewable and nonrenewable energy use in developing economies of Asia. *Renew. Energy* **2019**, *143*, 586–595. [Google Scholar] [CrossRef]
3. International Energy Agency (IEA). *Global Energy and Carbon Emissions Report*; International Energy Agency: Paris, France, 2020. [Google Scholar]
4. Fan, H.; Yu, Z.; Xia, S.; Li, X. Review on coordinated planning of source-network-load-storage for integrated energy systems. *Front. Energy Res.* **2021**, *9*, 641158. [Google Scholar] [CrossRef]
5. Zeng, L.; Wang, J.; Zhao, L. An inter-provincial tradable green certificate futures trading model under renewable portfolio standard policy. *Energy* **2022**, *257*, 124772. [Google Scholar] [CrossRef]
6. Gao, J.; Meng, Q.; Liu, J.; Wang, Z. Thermoelectric optimization of integrated energy system considering wind-photovoltaic uncertainty, two-stage power-to-gas and ladder-type carbon trading. *Renew. Energy* **2024**, *221*, 119806. [Google Scholar] [CrossRef]
7. Yang, D.; Liu, H.; Sun, Y.; Li, B.; Liu, C.; Liu, X. Mul-ti-agent joint peak regulation optimal scheduling con-sidering green certificate trading mechanism and deep peak regulation compen-sation for carbon capture power plant. *Power Syst. Technol.* **2024**, *48*, 100–112. (In Chinese) [Google Scholar]

8. Li, Y.; Wang, W.; Kou, Y.; Zhu, S. Considering green certificate-carbon joint trading and demand response integrated energy system economic operation. *Acta Energiae Solaris Sin.* **2023**, *44*, 538–546. (In Chinese) [Google Scholar]
9. Qin, J.; Pan, X.; Sun, X.; Guo, J.; Shi, W. Two-stage ro-bust optimization scheduling of integrated energy system and influence of repeated benefit under carbon-green certificate joint trading. *Electr. Power Autom. Equip.* **2024**, *44*, 59–67. (In Chinese) [Google Scholar]
10. Zhang, L.; Liu, D.; Cai, G.; Lyu, L.; Koh, L.H.; Wang, T. An optimal dispatch model for virtual power plant that incorporates carbon trading and green certificate trading. *Electr. Power Energy Syst.* **2023**, *144*, 108558. [Google Scholar] [CrossRef]
11. Yu, G.; Zhang, Z.; Cui, G.; Dong, Q.; Wang, S.; Li, X.; Shen, L.; Yan, H. Low-carbon economic dispatching strategy based on feasible region of cooperative interaction between wind-storage system and carbon capture power plant. *Renew. Energy* **2024**, *228*, 120706. [Google Scholar] [CrossRef]
12. Liang, T.; Chai, L.; Tan, J.; Jing, Y.; Lv, L. Dynamic optimization of an integrated energy system with carbon capture and power-togas interconnection: A deep reinforcement learning-based scheduling strategy. *Appl. Energy* **2024**, *367*, 123390. [Google Scholar] [CrossRef]
13. Luo, Z.; Yang, L.; Wang, H.; Zhang, Y.; Shen, X.; Zheng, L. Optimization and scheduling of integrated energy system with carbon capture powewr plant, electricity to gas and liquefied natural gas synergy. *Acta Energiae Solaris Sin.* **2025**, *46*, 438–448. (In Chinese) [Google Scholar]
14. Liu, X.; Nie, F.; Yang, D.; Wang, Y.; Xu, Y. Low-carbon economic dispatch of integrated energy systems considering green certificates-carbon trading mechanisms under CCPP-P2G joint operation model. *Power Syst. Technol.* **2023**, *47*, 2207–2222. (In Chinese) [Google Scholar]
15. Wang, S.; Yin, S.; Bai, H. Introduction and efficiency evaluation of multi-storage regional integrated energy system considering optimal operation integrated demand side response. *IOP Conf. Ser. Earth Environ. Sci.* **2021**, *631*, 012109. [Google Scholar] [CrossRef]
16. Yang, H.; Li, M.; Jiang, Z. Multi-time scale optimal scheduling of regional integrated energy systems considering integrated demand response. *IEEE Access* **2020**, *8*, 5080–5090. [Google Scholar] [CrossRef]
17. Yang, X.; Deng, Y.; Wang, X.; Deng, F.; Zhang, Z.; Mei, L. Lowcarbon economic dispatch of regional comprehensive energy system with CHP-CCS-P2G coupling based on carbon trading-green certificate joint trading mechanism. *Acta Energiae Solaris Sin.* **2024**, *45*, 244–254. (In Chinese) [Google Scholar]
18. Yu, X.; Hu, Z.; Cheng, J.; Yan, G.; Gong, H.; Wu, J. Optimal dispatch of integrated energy system considering P2G-CCS and supply-demand flexible response under stepped carbon. *Eng. J. Wuhan Univ.* **2024**, *57*, 1360–1371. [Google Scholar]
19. Wu, H.; Liu, Z.; He, Y.; Ding, M.; Xu, B.; Zhang, M. Two-layer optimal scheduling method for regional integrated energy system considering flexibility characteristics of CHP system. *Energy* **2024**, *308*, 132970. [Google Scholar] [CrossRef]
20. Gao, C.; Liu, J.; Zeng, J.; Han, F. Wind-photovoltaic co-generation prediction and energy scheduling of low-carbon complex regional integrated energy system with hydrogen industry chain based on copula-MILP. *Appl. Energy* **2022**, *328*, 120205. [Google Scholar] [CrossRef]
21. Zhu, X.; Xue, J.; Hu, M.; Liu, Z.; Gao, X.; Huang, W. Low-carbon econo-my dispatching of integrated energy system with P2G-HGT cou-pling wind power absorption basedon stepped carbon emission trading. *Energy Rep.* **2023**, *10*, 1753–1764. [Google Scholar] [CrossRef]
22. Zhang, J.; Liu, Z. Low carbon economic scheduling model for a park integrated energy system considering integrated demand response, ladder-type carbon trading and fine utilization of hydrogen. *Energy* **2024**, *290*, 130311. [Google Scholar] [CrossRef]
23. Chen, X.; Cao, X.; Chen, J.; Liu, J.; Zhang, Y.; Bao, H. Optimized Dispatch of Park Integrated Energy System with ThermoelectricFlexible Response under Green Certificate-Carbon Trading Mechanism. *Electr. Power* **2024**, *57*, 110–120. (In Chinese) [Google Scholar]
24. Fan, S.; Zhang, J.; Yan, R.; He, Y.; Liu, Y.; Ye, Y. Optimal sched-uling of HIES considering green-certificate–carbon trading and flexible output of heat and power. *Electr. Power Eng. Technol.* **2025**, *44*, 86–96. (In Chinese) [Google Scholar]

Disclaimer/Publisher's Note: The statements, opinions and data contained in all publications are solely those of the individual author(s) and contributor(s) and not of MDPI and/or the editor(s). MDPI and/or the editor(s) disclaim responsibility for any injury to people or property resulting from any ideas, methods, instructions or products referred to in the content.